Processing and Application of Ceramics 9 [1] (2015) 33–42
DOI: 10.2298/PAC1501033S

Effects of Sr^{2+} doping on the electrical properties of $(Bi_{0.5}Na_{0.5})_{0.94}Ba_{0.06}TiO_3$ ceramics

Amrita Singh[1], Kamal Prasad[2], Ashutosh Prasad[1,*]

[1]*University Department of Physics, T.M. Bhagalpur University, Bhagalpur 812007, India*
[2]*Aryabhatta Centre for Nanoscience and Nanotechnology, Aryabhatta Knowledge University, Patna 800001, India*

Received 26 December 2014; Received in revised form 4 March 2015; Accepted 23 March 2015

Abstract

The influence of $SrTiO_3$ addition on the microstructure and various electrical properties of $(Bi_{0.5}Na_{0.5})_{0.94}Ba_{0.06}TiO_3$ (BNTBT6) ceramics, fabricated by a conventional high temperature solid state reaction, was investigated. Analysis of X-ray diffraction patterns revealed the formation of phase pure materials with tetragonal unit cell structure, tetragonality parameter c/a in the interval from 0.9940 to 1.0063 and crystallite sizes ranging from 33–76 nm for addition of 0.2 to 1 wt.% of $SrTiO_3$. SEM studies indicated that Sr^{2+} doping led to decrease in grain size and non-homogeneity of grain distribution for higher $SrTiO_3$ amount (>0.6 wt.%). Complex impedance, modulus, and conductivity studies indicated the presence of grains and grain boundary contribution, non-Debye type of relaxation and NTCR behaviour of the test ceramic samples. Temperature dependent real part of complex permittivity showed peaks at 475 °C and the dielectric loss tangent showed peaks corresponding to 125 °C and 475 °C for almost all compositions. AC activation energies, computed using Arrhenius relation in the temperature range of 325–500 °C for the BNTBT6 ceramic compositions having $SrTiO_3$ concentration from 0.2 to 1.0 wt.%, were seen to have maximal values at the lowest measurement frequency. Amongst the different chosen doped BNTBT6 ceramic compositions, the composition having 0.6 wt.% of $SrTiO_3$ showed the best ferroelectric and piezoelectric response with maximum value of P_r (8.24 μC/cm^2), minimum value of E_c (5.73 kV/mm) and maximum d_{33} value (~46 pC/N).

Keywords: *$(Bi_{0.5}Na_{0.5})_{0.94}Ba_{0.06}TiO_3$, morphotropic phase boundary, complex permittivity, AC conductivity, activation energy*

I. Introduction

During the last few decades, a remarkable progress in the field of piezoelectric materials has occurred in the direction towards the study of lead-free compositions with a view to find viable alternatives for conventional lead-based compounds which are hazardous and eco-unfriendly. For example, $Pb(Zr,Ti)O_3$ ceramics, containing at least 60 wt.% of toxic lead oxides, have constantly been used commercially in electrical and electronic devices for almost half a century due to their excellent dielectric properties. They are still the main piezoelectric materials for various actuator, sensor and transducer applications [1]. These lead-containing materials have been causing serious problems to the environment during manufacturing at high temperature or during disposal after usage. Thus, a lot of attempts have been made on the research and development of high performance lead-free piezoelectric ceramics or single crystals. Bismuth layer (BL) structured and tungsten bronze (TB) type oxides have their own disadvantages as compared to perovskite type ferroelectrics, such as difficult sintering (TB type oxides) or electric poling (BL type oxides) due to a big structural anisotropy [2–4]. Therefore, perovskite ferroelectrics are usually preferentially chosen as lead-free candidate materials. $Bi_{0.5}Na_{0.5}TiO_3$ (BNT) and $Na_{0.5}K_{0.5}NbO_3$ (NKN) are currently two main lead-free piezoelectric compositions with perovskite structures which have been investigated as alternative compounds [5]. Although NKN-based compositions exhibit better piezoelectric and electromechanical properties [6–8], the BNT-based lead-free ce-

* Corresponding author: tel: +916412501699
e-mail: *apd.phy@gmail.com*

ramics or single crystals have been commercially used for some applications because the latter possesses a relatively mature processibility and stable electrical properties. On the contrary, the NKN-based compositions show some problems in sintering, control of processing, durability against water, and reproducibility and stability of piezoelectric properties [5,9–12]. Therefore, a lot of modifications have to be done before their final application. BNT has been widely investigated and was considered to be a potential lead-free candidate material ever since it was discovered by Smolenskii *et al.* in 1960 [13]. It is a monoclinic perovskite ferroelectric with a relatively large remnant polarization, P_r = 38 μC/cm^2. However, because of its high coercive field, E_c = 73 kV/cm, and relatively high conductivity, the pure BNT is difficult to be poled and is not a good piezoelectric material. These problems were then circumvented, of course to a smaller extent, by forming solid solutions with $BaTiO_3$ (BT), $Bi_{0.5}K_{0.5}TiO_3$, $KNbO_3$, $NaNbO_3$, $(Sr_{1-x-y}Pb_xCa_y)TiO_3$, $BiFeO_3$, $BiScO_3$, etc. [14–21]. Among these systems, BNT-BT seems to be the most interesting one. In this system a morphotropic phase boundary (MPB) was found at 6 mol% of $BaTiO_3$ (0.94BNT-0.06BT), where the materials show enhanced dielectric, piezoelectric and electromechanical performances. Takenaka *et al.* as well as some other researchers [14–21] reported that 0.94BNT-0.06BT ceramics have relatively good properties such as: k_{33} = 0.55, k_{31} = 0.19, d_{33} = 125 pC/N and d_{31} = 40 pC/N. These properties were furthermore improved by a few research groups [14,22,23]. However, this material system has a high coercive electric field and moderate piezoelectric constants. It was believed that aliovalent substitution either at A- or B- site may induce soft or hard properties in a piezoelectric material by forming cation vacancies or oxygen vacancies, respectively. Several kinds of cations like Ce^{2+}, La^{3+}, Nb^{5+}, Co^{3+}, Mn^{2+}, Y^{3+} etc. were tested to further modify BNT-based lead-free piezoelectric ceramics [24–27]. Literature survey revealed that no systematic study, except that by Chen *et al.* [28], on the effect of Sr^{2+} doping on the dielectric, ferroelectric, and piezoelectric properties of 0.94BNT-0.06BT (BNTBT6), has been reported. It is why in this study, the influence of small amount of strontium addition on the structure, microstructure, dielectric, ferroelectric, AC conductivity, complex impedance, and piezoelectric properties in 0.94BNT-0.06BT compositions are discussed.

II. Experimental procedure

Polycrystalline $(Na_{1/2}Bi_{1/2})_{0.94}Ba_{0.06}TiO_3$ ceramics with addition of 0.2 to 1 wt.% of $SrTiO_3$ (denoted as BNTBT6-xST, where x = 0.2, 0.4, 0.6, 0.8 and 1), were prepared by a standard high-temperature solid-state reaction technique using AR grade (purity more than 99.5%, Hi-Media) oxides and/or carbonates: Bi_2O_3, Na_2CO_3, $SrTiO_3$, $BaCO_3$ and TiO_2 in suitable stoichiometric proportions. The above ingredients were mixed thoroughly, first in air and then in methanol medium, using agate mortar and pestle. This mixture was calcined at an optimized temperature of 1170 °C for about 3 h (to ensure the formation of pure perovskite phase) in a covered AR-grade alumina crucible. Then, by adding a small amount of polyvinyl alcohol (PVA) as binder to the calcined powder, circular and rectangular disc shaped pellets having thickness in the range of 1–2 mm were fabricated by applying uniaxial pressure of 6 tons/square inch on the powders. The pellets were subsequently sintered at the optimized temperature of 1175 °C in air atmosphere for about 2 h to achieve maximum density (~95% of the theoretical density).

The XRD patterns of BNTBT6-xST powders (where x = 0.2, 0.4, 0.6, 0.8 and 1) were obtained from an X-ray diffractometer (X'pert-PRO, Pan Analytical, USA), using Cu K_α radiation (λ = 1.5405 Å) over a wide range of Bragg angles ($20° \leq 2\theta \leq 80°$) at the room temperature. A standard computer program POWD-X was utilized for the XRD-profile analysis. Surface morphology of the sintered samples was examined by a scanning electron microscope (JEOL-JSM840A). The frequency and temperature dependent dielectric constant (ε_r), loss tangent ($\tan\delta$), complex impedance (Z^*) and phase angle (θ) were measured using a computer-controlled LCR Hi-Tester (HIOKI 3532-50, Japan) on a symmetrical cell consisting of Ag|ceramic|Ag, where Ag is a conductive paint coated on each side of the pellet. Longitudinal piezoelectric charge coefficients (d_{33}) of all the poled ceramic samples were measured using a PM3500 d_{33}/d_{31} meter (KCF Technologies, USA) under an applied DC electric field of about 1.5 kV/mm at 80 °C in a silicone oil bath for about 15 minutes.

III. Results and discussion

3.1. Structural study

XRD patterns of the calcined BNTBT6-xST powders (where x = 0.2, 0.4, 0.6, 0.8 and 1) are presented in Fig. 1a while Fig. 1b shows the fine scanning in the 2θ range of 46.0–47.5° for the ceramics sintered at 1175 °C. A small shift of the diffraction peaks can be seen in the samples with addition of $SrTiO_3$. Thus, XRD data analysis shows that Sr^{2+} can diffuse into the lattice of BNTBT6 ceramics. Good agreement between the observed and calculated inter-planar spacing without any trace of extra peaks due to secondary phases pertaining to the constituent oxides suggested the formation of a single-phase compound with tetragonal structure. The possible incorporation of Sr^{2+} at the A-site in the complex ABO_3 type oxide of the investigated ceramic compositions may distort the unit cell, change the dipolar moment, and induce strain in the lattice because of more cations co-occupying the same lattice of unit cell. In addition, Sr^{2+} doping may result in inhomogeneous crystal structure at the nanometre scale and therefore a more relaxation-like response can be expected.

Table 1 enlists the values of unit cell parameters,

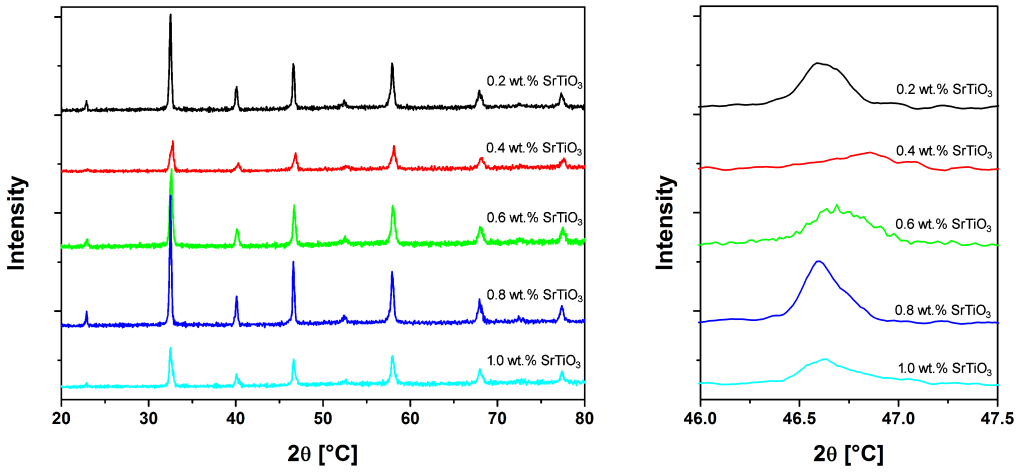

Figure 1. XRD patterns of BNTBT6 having different fractions of $SrTiO_3$ recorded in 2θ interval: a) 20–80° and b) 46.0–47.5°

tetragonality parameter and volume of unit cell of BNTBT6-xST ceramics having different fractions of $SrTiO_3$ in the compositions. Analysis of X-ray diffraction patterns revealed the formation of phase pure materials with tetragonal unit cell structure, tetragonality parameter c/a attaining maximum and minimum values equal to 1.0063 and 0.9940 for 0.4 and 0.8 mol% of $SrTiO_3$, respectively.

3.2. Microstructural study

Figure 2 shows the SEM micrographs of BNTBT6-xST ceramics in which grainy structure is clearly visible, thereby indicating the existence of polycrystalline microstructure. Grains of slightly unequal sizes appear to be distributed throughout the samples. Table 2 enlists the grain sizes in the pure BNTBT6 and compositions having different fractions of $SrTiO_3$ and it can be seen that the average grain size was estimated to be ~1.22–3.74 μm. Apparent densities of all sintered ceramics were found to be ~95% of the corresponding theoretical ones. SEM micrographs (and data in Table 2) indicated that substitution of Sr^{2+} for Ba^{2+} at the A-site led to decrease in grain size with the increase of $SrTiO_3$ content. Thus, $SrTiO_3$ doping in small proportion is seen to produce a significant influence on sintering of BNTBT6 ceramics. However, excessive $SrTiO_3$ doping beyond 0.6 wt.% led to non-homogeneity of grain distribution, probably associated to the pinning effect of grain boundary owing to segregation of some smaller sized particles. Those structural changes might be caused by Sr^{2+} (ionic radius = 1.18 Å) substituting the larger Ba^{2+} ions (ionic radius = 1.35 Å) mostly in the grain boundary area and/or donor ions formed owing to the substitution of Sr^{2+} for smaller sized Na^+ (radius = 1.02 Å) and Bi^{3+} (radius = 1.03 Å). Thus, Sr^{2+} may act as a donor and hence as a softener that may lead to some Na-site vacancies which would relax the strain caused by reorientation of domains. Therefore, the movement of the domains becomes easier and, thus, electrical properties of the BNTBT6 ceramics are expected to improve significantly by Sr^{2+} doping. Doping with $SrTiO_3$ in suitable proportion might have led to an increase in unit cell volume, lower c/a values etc., thus, corroborating the results derived from structural study on the powder ceramic samples. The slight distortion of the unit cell was attributed to larger sized Sr^{2+} ions diffused into the BNTBT6 lattice to replace Bi^{3+}, Na^+ resulting in the enlargement of lattice constant and lattice energy which tends to promote a phase transformation in order to stabilize the structure.

3.3. Dielectric study

It is expected that the dopant in the base BNTBT6 material can modify the dielectric properties in various ways and create a material with a desired response. Figures 3a and 3b depict temperature dependence of real

Table 1. Unit cell parameters, tetragonality parameter and volume of unit cell in BNTBT6-xST having different fractions of $SrTiO_3$

Fractions of $SrTiO_3$ in BNTBT6-xST	a [Å]	c [Å]	c/a	V [Å^3]
0.002	3.8815	3.8623	0.995	58.19
0.004	3.8736	3.8978	1.0063	58.48
0.006	3.8797	3.8566	0.9941	58.05
0.008	3.8856	3.8623	0.994	58.31
0.010	3.8856	3.8935	1.002	58.78

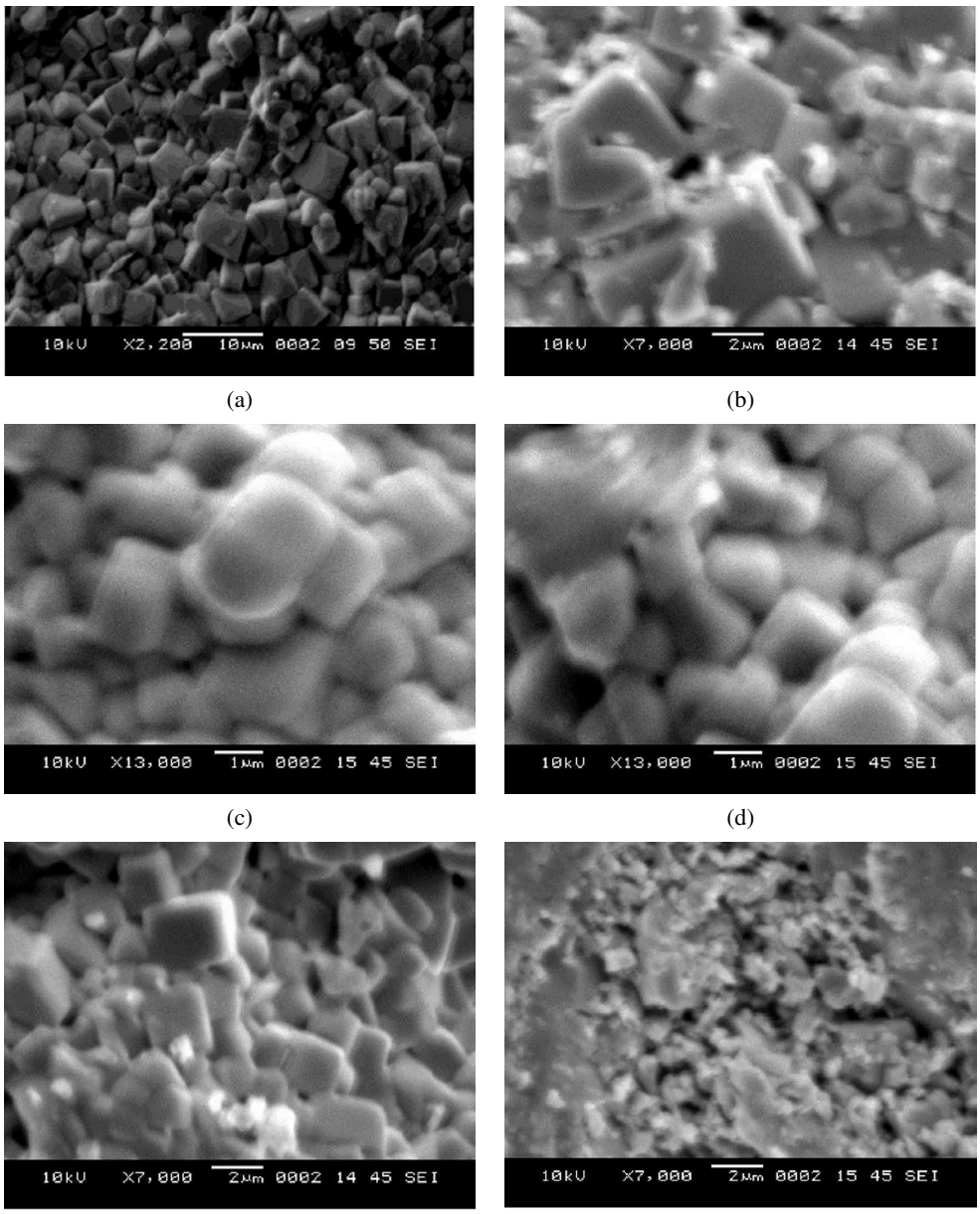

Figure 2. SEM micrographs of BNTBT6-xST having different fractions of $SrTiO_3$: a) 0, b) 0.2, c) 0.4, d) 0.6, e) 0.8 and f) 1 wt.%

Table 2. Grain sizes in BNTBT6 and in BNTBT6-xST having different fractions of $SrTiO_3$

Fractions of $SrTiO_3$ in BNTBT6-xST	Grain size [μm]
0	3.01
0.002	2.95
0.004	3.74
0.006	1.70
0.008	1.64
0.010	1.22

part (ε') of complex permittivity at 1 kHz frequency and frequency dependence of ε' at the ambient temperature (35 °C), respectively, for Sr^{2+} doped BNTBT6 samples. The dielectric constant versus temperature curves (Fig. 3a) exhibit peaks almost at a fixed Curie temperature (T_m ~ 475 °C), independent of the amount of Sr^{2+} doping. As depicted in Fig. 3b, at room temperature maximal and minimal values of dielectric constant for Sr^{2+} doped BNTBT6 samples at 100 Hz are ~4038 and 1231 for 0.2 and 1 wt.% of Sr^{2+} doped BNTBT6 samples, respectively. $\varepsilon'(\omega)$ is seen to provide a monotonic decrease with increasing frequency and the decrease of ε' with frequency is greater at higher temperatures. The higher ε' values at lower frequencies for polar materials are attributed to the contribution of multi-component polarization mechanisms (i.e. electronic, ionic, orientation and space charge). At higher frequencies the dipoles cannot rotate rapidly, so that their oscillations lag behind those of the field. As the frequency is further raised, the dipoles are completely unable to follow the

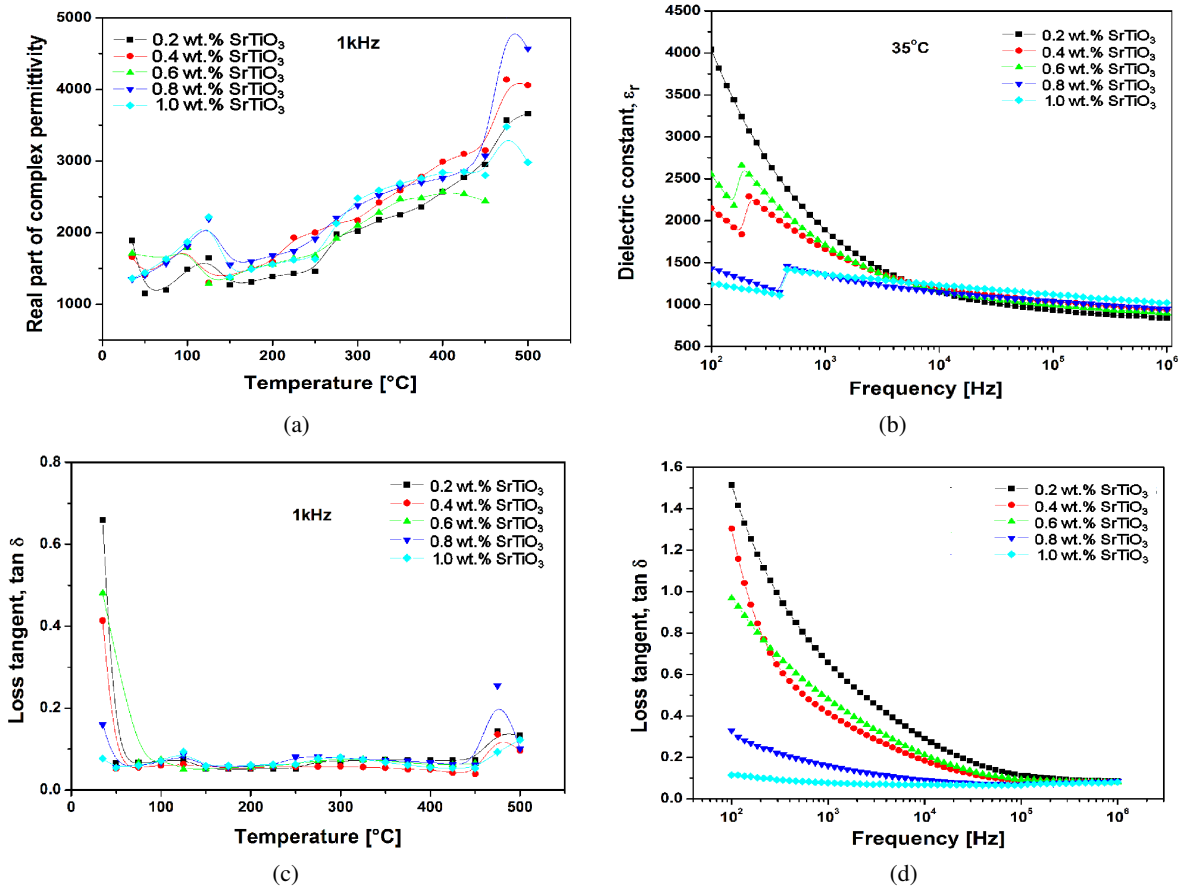

Figure 3. Temperature and frequency dependence of dielectric constant (a and b) and dielectric loss tangent (c and d) for BNTBT6-xST ceramics

field and hence the orientational polarization ceases, so ε' decreases and attains a constant value at higher frequencies (~1 MHz) that is attributed to the interfacial polarization [31]. This variation of ε' with frequency can be explained on the basis of Maxwell-Wagner two-layers model for space charge or interfacial polarization with Koop's phenomenological theory [32,33]. According to this model, dielectric materials are supposed to consist of large number of well conducting grains which are separated by poorly conducting thin grain boundaries. Under the application of external electric field, the charge carriers can easily migrate from the grains and get accumulated at the grain boundaries. This process can produce large polarization and high dielectric constant. The decrease of ε' with frequency arises from the fact that because of inertia, the polarization does not occur instantaneously with the application of the electric field. The delay in response towards the applied alternating electric field leads to the consequent decrease in dielectric constant. Also, at lower frequencies, all four types of mechanism for polarization contribute to the total polarization of the material and hence higher value of dielectric constant arises. With the increase in frequency, the dipoles with large relaxation times cease to respond to the applied frequency and hence decrease in the dielectric constant is caused. This type of frequency dependence of dielectric behaviour is found in many ferroelectric materials [34,35]. As shown in Fig. 3b, at a fixed frequency (100 Hz, 1 kHz and 10 kHz) the values of ε' are seen to decrease proportionately with the increase of Sr^{2+} content, except for the composition having 0.4 wt.% of Sr^{2+} which shows the opposite trend of variation. Above 10 kHz, an exactly opposite dielectric dispersion is observed. This can also be explained on the basis of Maxwell-Wagner theory. According to this theory, the dielectric constant is directly proportional to the grain size of the samples [36] and the sharp decrease of grain sizes is seen for the samples with Sr^{2+} content up to 0.6 wt.% (Fig. 2, Table 2).

Figures 3c and 3d depict the temperature dependence of dielectric loss tangent ($\tan\delta$) at 1 kHz and frequency dependence of the same parameter at the ambient temperature (35 °C) for Sr^{2+} doped BNTBT6 samples, respectively. The loss tangent versus temperature curves (Fig. 3c) exhibit peaks almost at a fixed temperature (T_m ~ 475 °C, at which the ferroelectric-paraelectric phase transition is supposed to take place) for all Sr^{2+} doped BNTBT6 samples. Further, as depicted in Fig. 3d, the values of $\tan\delta$ for Sr^{2+} doped BNTBT6 samples are seen to decrease with frequency up to 100 kHz and at about 1 MHz all curves are merged together to attain minimal values (~0.08–0.11). This can again be explained in the light of Maxwell-Wagner theory which endorses the existence of peaks

in the temperature-dependent loss function [37]. The temperature-dependent dielectric loss tangent ($\tan\delta$) is owed to the relaxation of space charge polarization [38].

3.4. Impedance study

Figures 4a and 4b show the $Z'(f)$ and $Z''(f)$ plots for BNTBT6-xST ceramics at the ambient temperature, respectively. At 100 Hz the maximal and minimal values of Z' are ~1.056 MΩ and 0.4 MΩ for the composition having 0.4 and 1 wt.% of $SrTiO_3$ doping in BNTBT6, respectively. The corresponding maximal and minimal values of Z'' are ~3.6 MΩ and 0.3 MΩ for the compositions having 1 and 0.4 wt.% of $SrTiO_3$ doping in BNTBT6. As shown in Fig. 4a, the frequency-independent minimal magnitude of Z' is ~57 kΩ, common to all doped ceramic compositions at the ambient temperature. From the plots it is seen that at low temperature, Z' decreases monotonically with increasing frequency up to a certain limiting range (~10 kHz) above which it becomes almost frequency- independent. The higher values of Z' at lower frequencies indicate that the polarization in the investigated ceramics is large. This signifies that the grain boundaries are not relaxing even at the highest measurement frequency. $Z''(f)$ plots (shown in Fig. 4b) indicate almost identical monotonically decreasing type of variation up to the same frequency limit ~10 kHz beyond which they merge together at a very low value of Z'' to show frequency-independent nature of variation extending up to the highest frequency limit at all the chosen doping concentrations of Sr^{2+}. It is also seen that the nature of variation of Z'' with frequency is opposite to that of Z' for all doped ceramic compositions. The merging of Z'' (as well as of Z') at higher frequencies indicates possible release of space charge accumulation at the boundaries of homogeneous phases in the test material under the applied external field. At the ambient temperature monotonic decrease of Z'' for all the compositions indicated that at lower temperatures the relaxation is absent in the investigated materials. This means that in the prepared samples relaxation species are immobile defects and only the orientation effects may be associated. Also, the decreasing magnitudes of Z' and Z'' with increasing frequencies implied that relaxation in the material is temperature-dependent, and apparently there is no single relaxation time.

3.5. Complex impedance/modulus spectroscopy

Complex impedance spectroscopy (CIS) is a powerful tool for characterizing many of the electrical properties of materials and their interfaces with electronically conducting electrodes. The CIS gives a direct correlation between the response of a real system and an idealized model circuit composed of discrete electrical components. It may be used to investigate the dynamics of bound or mobile charges in the bulk or interfacial regions of any kind of solid or liquid material: ionic, semiconducting, mixed electronic-ionic and even insulators (dielectrics). Most of real ceramics contain grains and grain boundary regions, which individually have very different physical properties. These regions are well observed in the impedance and modulus spectra. The electrical properties of the prepared ceramic samples have been investigated using CIS as well as complex modulus spectroscopy (CMS) techniques. Electrical AC data may be presented in any of four interrelated formalism: relative permittivity $\varepsilon^* = \varepsilon' - j\varepsilon''$; impedance $Z^* = Z' + jZ'' = 1/j\omega C_0\varepsilon^*$; electric modulus $M^* = M' + jM'' = 1/\varepsilon^*$; admittance $Y^* = Y' + jY'' = j\omega C_0\varepsilon^*$; and $\tan\delta = \varepsilon''/\varepsilon' = M''/M' = Z'/Z'' = Y''/Y'$, where ω ($= 2\pi f$) is the angular frequency, $C_0 = \varepsilon_0 A/d$ is the geometrical capacitance, $j = \sqrt{-1}$; ε_0 is the permittivity of free space, 8.854×10^{-12} F/m; d and A are the thickness and area of the pellet, respectively, and δ is complementary to the phase angle, θ, as observed by the LCR Hi-Tester. To study the contribution of various microscopic elements, such as intragrain, intergrain, electrode effect, and relaxation process, Cole-Cole plot

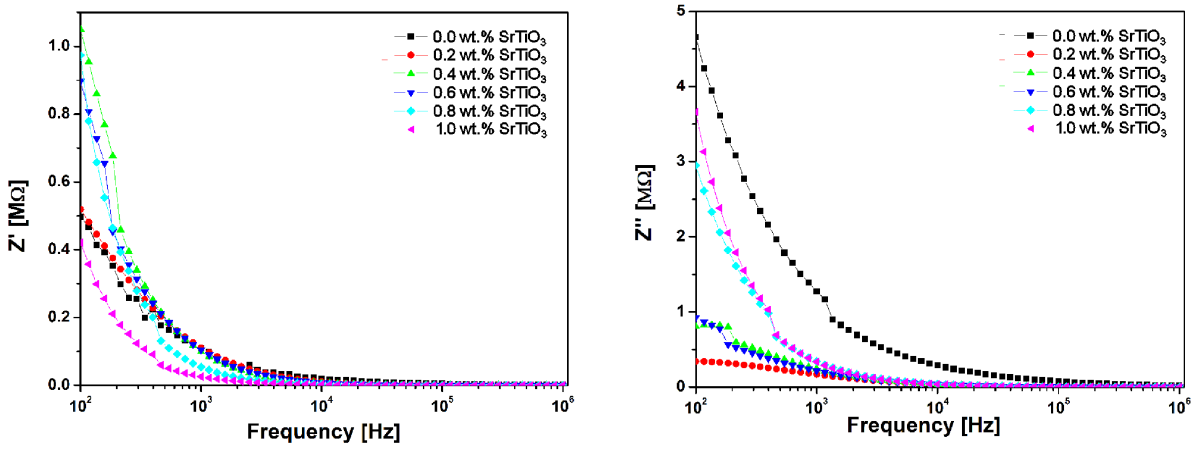

(a) (b)

Figure 4. Frequency dependence of real (a) and imaginary parts (b) of complex impedance (Z^*) for BNTBT6-xST ceramics at room temperature

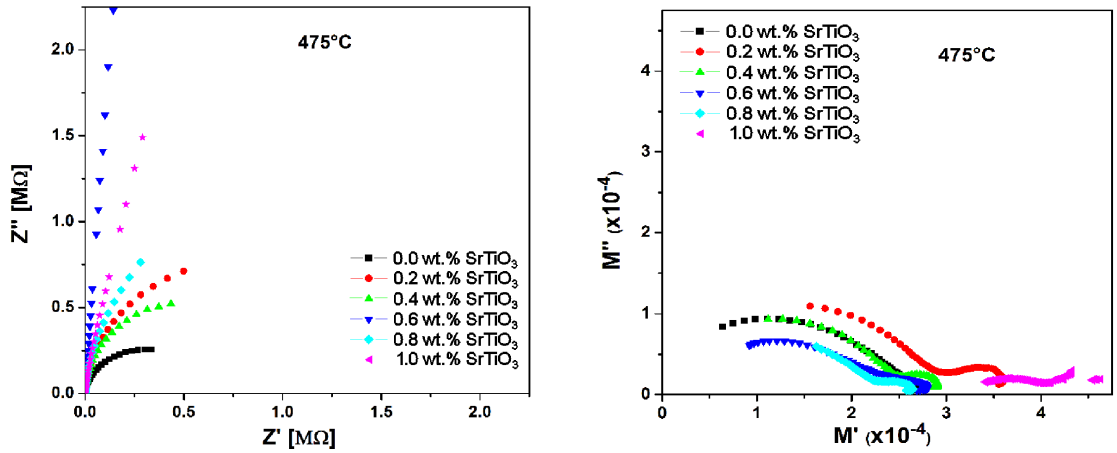

(a) (b)

Figure 5. Complex impedance (a) and modulus plots (b) for for BNTBT6-xST ceramics, measured at 475 °C

analysis was used. Figure 5a shows the Cole-Cole plots of the compounds corresponding to 475 °C as the measurement temperature in which it is observed that the composition having 0.6 wt.% Sr^{2+} dopant has very high order of insulating properties because they provide plots in the form of almost straight lines parallel to the ordinate. However, the resulting curves for the other Sr^{2+} dopant contents showed a tendency to bend towards the abscissa to form semicircles with their centres below the real axis, having comparatively larger radii and the radii decreasing with the increase of temperature, thereby indicating negative temperature coefficient of resistivity (NTCR) behaviour of the materials, generally found in case of semiconductors, showing a clear-cut departure from the ideal Debye type behaviour. This non-ideal behaviour could be attributed to several factors such as grain orientation, grain boundary, stress-strain phenomena, and atomic defect distribution. A series array of two parallel RC combinations $[(R_g, C_g), (R_{gb}, C_{gb})]$ in series with a resistor (R_s) indicate the contribution from grains of the sample in the high frequency region and from the grain boundaries in the low frequency region. No other relaxation mechanism, such as the electrode effects, could be identified through the use of CIS technique in the test frequency and temperature range.

The impedance data could be analysed in a much better way by re-plotting the data in the complex modulus (M^*) formalism, which is based on the polarization analysis. The dopant (Sr^{2+}) concentration dependence of the complex modulus spectrum ($M''(f)$ vs. $M'(f)$) for the doped BNTBT6 ceramic compositions corresponding to 475 °C as the measurement temperature is shown in Fig. 5b. From this figure, we can notice that the samples' modulus spectrum has a typical semicircular pattern with its centre lying below the real axis, thereby indicating non-Debye type of relaxation response in the investigated material system. The main difference from the corresponding complex impedance plots (as illustrated in Fig. 5a) is that in the case of modulus plots (Fig. 5b), the depressed semicircles corresponding to grains and grain boundaries are clearly visible and well separated whereas in the impedance spectra they almost overlaps. In the modulus spectrum, right semicircles represent data corresponding to higher frequencies and left semicircles represent data corresponding to lower frequencies for each set. Larger semicircles for the grain-boundaries and smaller ones for the grains in each of the plots in Fig. 5b show the dominance of grain-boundaries over the grains in each of the given compositions at the test measurement temperature (475 °C).

3.6. Electrical conductivity

The real part of AC conductivity (σ'_{AC}) is directly related to the dielectric properties of the material: the real part of the dominant bulk conductivity may be evaluated from the impedance spectrum using the relation $\sigma'_{AC} = t/(Z'A)$, where $Z'(= Z^* \cos\theta)$ is the real part of complex impedance; t is the thickness; θ is the phase angle and A the surface area of the sample. Approximate values of DC conductivity of the test materials were evaluated from the extrapolation of the available plateaus of the $\sigma_{AC}(\omega)$ plots down to $\omega = 0$ for all Sr^{2+} doped BNTBT6 ceramic compositions in view of the fact that the frequency-dependent AC conductivity is given by the relation [39–43]:

$$\sigma = \sigma_0 + A\omega^{S_1} + B\omega^{S_2} \tag{1}$$

in which A, B, S_1 and S_2 are constants and $\omega = 2\pi f$ (f being the frequency) is the angular frequency. The AC conductivity-based activation energy was obtained using the Arrhenius relationship:

$$\sigma_{AC} = \sigma_0 \exp\left(\frac{-E_a}{k_B T}\right) \tag{2}$$

Thus, it is clear that the slope of the $\ln(\sigma_{AC})$ vs. $10^3/T$ plots would yield the values of activation energy for AC conductivity (E_a). Figure 6 shows the frequency-dependence of real part of complex AC conductivity (σ'_{AC}) for BNTNT6-xST ceramics at the room temperature and Fig. 7 shows the inverse temperature depen-

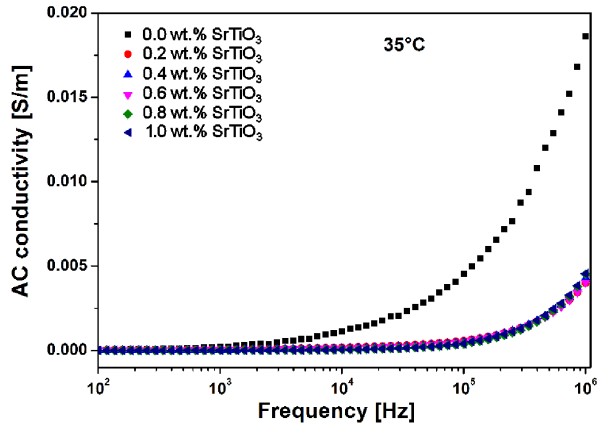

Figure 6. Frequency dependence of real part of complex AC conductivity (σ^*_{AC}) for BNTBT6-xST ceramics at room temperature

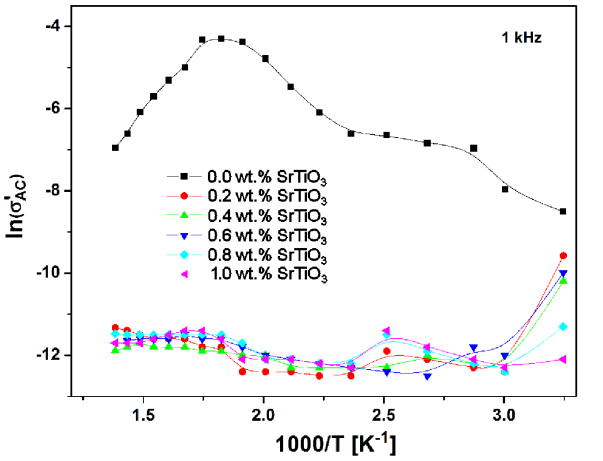

Figure 7. Inverse temperature dependence of log of real part of complex AC conductivity (σ^*_{AC}) for BNTBT6-xST ceramics at 1 kHz

dence of log of real part of complex AC conductivity (σ^*_{AC}) for the same Sr^{2+} doped BNTBT6 ceramic compositions at 1 kHz. From Fig. 6 it is apparent that for all doped BNTBT6 ceramic compositions (except the pure BNTBT6 ceramics) the AC conductivity is seen to have no role at least up to 10 kHz. On the other hand, for BNTBT6 ceramic sample, the AC conductivity is seen to no role even at the lowest frequency of measurement. The values of real part of AC conductivity at 1 kHz, 10 kHz, 100 kHz and 1 MHz are 9.3×10^{-5}, 1.55×10^{-4}, 6.3×10^{-4} and 4.1×10^{-3} S/m, respectively. As referred to earlier, a linear least squares fit of the conductivity data for BNTBT6-xST (x = 0, 0.2, 0.4, 0.6, 0.8 and 1) ceramic compositions to equation 2 gives the value of the apparent activation energy (E_a) for them. As it is evident from the plots in Fig 7, it may be inferred that real part of complex AC conductivity (σ'_{AC}) (and hence the value of the apparent activation energy, E_a) for BNTBT6 ceramic sharply rises up to the Curie temperature above which it goes down rapidly in the region of paraelectric phase of the ceramic. On the other hand, the Sr^{2+} doped BNTBT6 ceramic compositions do not show such sharp rise and fall of AC conductivity and the magnitudes of the computed apparent activation energies of all Sr^{2+} doped BNTBT6 ceramic compositions are comparatively smaller near the Curie point. Activation energy values are ~0.1469 eV, 0.048 eV, 0.1248 eV, 0.01716 eV and negligibly small for 0.2, 0.4, 0.6, 0.8 and 1 wt.% $SrTiO_3$ doped BNTBT6 ceramics, respectively. The enhancement in AC conductivity with temperature for 0.2, 0.4, 0.6, 0.8 and 1 wt.% of $SrTiO_3$ doped BNTBT6 ceramics (even may be small in magnitude) may be attributed to the fact that within the bulk, the oxygen vacancies are usually created during heat treatment due to the loss of oxygen are usually created during sintering and the charge compensation follows the Kröger-Vink equation [40]:

$$O_O \longrightarrow \tfrac{1}{2}O_2 \uparrow + V_O^{\bullet\bullet} + 2e^{-1} \qquad (3)$$

which shows that free electrons are left behind, making the n-type materials.

3.7. Piezoelectric and ferroelectric response

Longitudinal piezoelectric charge coefficient (d_{33}) of the poled (under an applied DC electric field of about 1.5 kV/mm at 80 °C in a silicone oil bath for about 15 minutes) doped BNTBT6 ceramic samples with 0.2, 0.4, 0.6, 0.8 and 1 wt.% of $SrTiO_3$ are found to be ~35, 33, 46, 28 and 19.5 pC/N, respectively.

Figure 8 shows dependence of polarization (P_r) and coercive field (E_c) on the $SrTiO_3$ doping concentration for the aforesaid compositions. It revealed that the BNTBT ceramic composition having 0.6 wt.% of $SrTiO_3$ provided comparatively the best ferroelectric response amongst the different tested doped BNTBT6 ceramic compositions with maximum value of P_r (= 8.24 μC/cm^2) and minimum value of E_c (= 5.73 kV/mm). From the comparison of our results for values of d_{33} and P_r with those reported in a

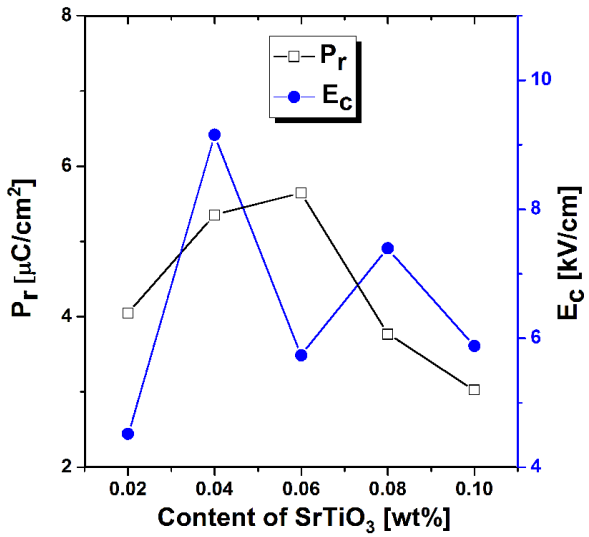

Figure 8. Dependence of polarization (P_r) and coercive field (E_c) on $SrTiO_3$ doping concentration for BNTBT6-xST ceramics at 1 kHz

recent literature [45] on similar material compositions, it transpires that our results certainly fall short of those reported in the literature. The obvious possible reasons for our samples having inferior properties are the following: (i) the Sr^{2+} doping in the present study has been enacted after the process of calcination i.e., only after the phase formation in BNTBT6 is over, whereas in the work referred to earlier [45] the dopant powder was introduced *ab initio* i.e., well before the process of calcination; (ii) the entire process of dry as well as wet mixing of the constituent powder compositions has been performed through conventional route i.e., by mortar and pestle and not through ball-milling or through chemical route which are certainly capable of producing highly dense and more homogeneous fine powder samples than those obtained through the conventional route as detailed above and (iii) a comparatively lower value of DC electric field strength could be applied over the fabricated samples in the present study because the samples were unable to withstand higher fields than 1.5 kV/mm due to the high leakage currents presumably owing to their comparatively larger porosities. On the other hand, in the referred literature and others [44,45] the applied field strength is ~4–7 kV/mm. Refinements in the method of fabrication of the ceramic samples are certainly expected to lead to the enhanced dielectric, piezoelectric, and ferroelectric properties in them.

IV. Conclusions

The effects of Sr^{2+} substitution on microstructure and various electrical properties (like frequency- and temperature-dependent complex permittivity, complex impedance, conductivity, ferroelectric, and piezoelectric properties) of the $(Bi_{0.5}Na_{0.5})_{0.94}Ba_{0.06}TiO_3$ (BNTBT6) ceramics were examined. X-ray diffraction patterns revealed the formation of phase pure materials with tetragonal unit cell structure without any secondary impurity phases. The dielectric, ferroelectric, and piezoelectric properties are improved obviously with the optimum values for BNTBT6 ceramic with 0.6 wt.% of $SrTiO_3$: ambient dielectric constant ~2700; minimum loss tangent ~0.08; d_{33} ~46 pC/N and $(E_c)_{min}$ ~5.73 kV/mm. These improved electrical properties of BNTBT6 ceramic sample with 0.6 wt.% of $SrTiO_3$ indicate its promising application in electronic devices. Complex impedance, modulus, and conductivity studies indicated the presence of grains and grain boundary contribution, non-Debye type of relaxation and NTCR behaviour of the test ceramic samples. AC activation energies in the temperature range of 325–500 °C provided maximal values for BNTBT6 composition having 0.6 wt.% of $SrTiO_3$.

Acknowledgement: The authors gratefully acknowledge the financial support by the Department of Science and Technology, New Delhi through Grant No.SR/S2/CMP-017/2008 under which the present work was undertaken.

References

1. B. Jaffe, W.R. Cook, H. Jaffe, *Piezoelectric Ceramics*, Academic Press, New York, 1971, pp. 115–181.
2. M. Suzuki, H. Nagata, J. Ohara, H. Funakubo, T. Takenaka, "$Bi_{3-x}M_xTiTaO_9$ (M = La or Nd) ceramics with high mechanical quality factor Q_m", *Jpn. J. Appl. Phys.*, **42** (2003) 6090–6093.
3. R.J. Xie, Y. Akimune, R. Wang, N. Hirosaki, T. Nishimuna, "Dielectric and piezoelectric properties of barium-substituted $Sr_{1.9}Ca_{0.1}NaNb_5O_{15}$ ceramics" *Jpn. J. Appl. Phys.*, **42** (2003) 7404–7409.
4. M.D. Maeder, D. Damjanovic, N. Setter, "Lead free piezoelectric materials", *J. Electroceram.*, **13** (2004) 385–392.
5. Y. Guo, K. Kakimoto, H. Ohsato, "Phase transitional behavior and piezoelectric properties of $Na_{0.5}K_{0.5}NbO_3$–$LiNbO_3$ ceramics", *Appl. Phys. Lett.*, **85** (2004) 4121–4123.
6. Y. Saito, H. Takao, T. Tani, T. Nonoyama, K. Takatori, T. Homma, T. Nagaya, M. Nakamura, "Lead free piezoceramics", *Nature*, **432** (2004) 84–87.
7. E. Hollenstein, M. Davis, D. Damjanovic, N. Setter, "Piezoelectric properties of Li- and Ta-modified $K_{0.5}Na_{0.5}NbO_3$ ceramics", *Appl. Phys. Lett.*, **87** (2005) 182905.
8. M. Matsubara, T. Yamaguchi, K. Kikuta, S. Hirano, "Sinterability and piezoelectric properties of (K,Na)NbO_3 ceramics with novel sintering aid", *Jpn. J. Appl. Phys.*, **43** (2004) 7159–7163.
9. M. Kosec, D. Kolar, "On activated sintering and electrical properties of $NaKNbO_3$", *Mater. Res. Bull.*, **10** (1975) 335–340.
10. R.R., Zeyfang, R.M. Henson, W.J. Maier, "Temperature- and time dependent properties of polycrystalline (Li,Na)NbO_3 solid solutions", *J. Appl. Phys.*, **48** (1977) 3014–3017.
11. J. Yoo, K. Lee, K. Chung, S. Lee, K. Kim, J. Hong, S. Ryu, C. Lhee, "Piezoelectric and dielectric properties of (LiNaK)(NbTaSb)O_3 ceramics with variation in poling temperature", *Jpn. J. Appl. Phys.*, **45** (2006) 7444–7448.
12. G.A. Smolenskii, V.A. Isupov, A.I. Agranovskaya, N.N. Krainik, "New ferroelectrics of complex composition", *Sov. Phys.-Solid State (Engl. Transl.)*, **2** (1961) 2651–2654.
13. T. Takenaka, K. Sakata, K. Toda, "Piezoelectric properties of $(Bi_{0.5}Na_{0.5})TiO_3$-based ceramics", *Ferroelectrics*, **106** (1990) 375–380.
14. T. Takenaka, K. Maruyama, K. Sakata, "$(Bi_{0.5}Na_{0.5})TiO_3$–$BaTiO_3$ system for lead free piezoelectric ceramics", *Jpn. J. Appl. Phys.*, **30** (1991) 2236–2239.
15. H. Nagata, T. Takenaka, "Lead free piezoelectric ceramics of $(Na_{0.5}Bi_{0.5})TiO_3$–$\frac{1}{2}(Bi_2O_3{\cdot}Sc_2O_3)$ system", *Jpn. J. Appl. Phys. Part 1*, **36** (1997) 6055–6057.
16. H. Nagata, T. Takenaka, "Lead-free piezoelectric ceramics of $(Na_{0.5}Bi_{0.5})TiO_3$–$KNbO_3$–

$\frac{1}{2}$ (Bi_2O_3·Sc_2O_3) system", *Jpn. J. Appl. Phys.*, **37** (1998) 5311–5314.
17. A. Sasaki, T. Chiba, Y. Mamiya, E. Otsuki, "Dielectric and piezoelectric properties of $(Bi_{0.5}Na_{0.5})TiO_3$–$(Bi_{0.5}K_{0.5})TiO_3$ systems". *Jpn. J. Appl. Phys.*, **38** (1999) 5564–5567.
18. H. Nagata, N. Koizumi, T. Takenaka, "Lead-free piezoelectric ceramics of $(Bi_{0.5}Na_{0.5})TiO_3$–$BiFeO_3$ system", *Key Eng. Mater.*, **169-170** (1999) 37–40.
19. T. Wada, K. Toyoike, Y. Imanaka, Y. Matsuo, "Dielectric and piezoelectric properties of $(A_{0.5}Bi_{0.5})TiO_3$–$ANbO_3$ (A = Na, K) systems", *Jpn. J. Appl. Phys.*, **40** (2001) 5703–5705.
20. Y.M. Li, W. Chen, Q. Xu, J. Zhou, H.J. Sun, M.S. Liao, "Dielecric and piezoelectric properties of $(Na_{0.5}Bi_{0.5})TiO_3$–$(K_{0.5}Bi_{0.5})TiO_3$–$NaNbO_3$ lead free ceramics", *J. Electroceram.*, **14** (2005) 53–58.
21. Y.G. Wu, H.L. Zhang, Y. Zhang, J.Y. Ma, D.H. Xie, "Lead free piezoelectric ceramics with composition of (0.97-x)$(Na_{0.5}Bi_{0.5})TiO_3$–0.03$NaNbO_3$–x$BaTiO_3$", *J. Mater. Sci.*, **38** (2003) 987–994.
22. W. Jo, J.E. Daniels, J.L. Jones, X. Tan, P.A. Thomas, D. Damjanovic, J. Rödel, "Evolving morphotropic phase boundary in lead-free $(Bi_{1/2}Na_{1/2})TiO_3$–$BaTiO_3$ piezoceramics", *J. Appl. Phys.*, **109** (2011) 014110-p1–7.
23. A.K. Roy, A. Singh, K. Kumari, K. Amar Nath, A. Prasad, K. Prasad, "Electrical properties and ac conductivity of $(Bi_{0.5}Na_{0.5})_{0.94}Ba_{0.06}TiO_3$ ceramic", *ISRN Ceramics*, **2012** (2012) 1–10.
24. H. Nagata, M. Yoshida, Y. Makiuchi, T. Takenana, "Large piezoelectric constant and high Curie temperature of lead-free piezoelectric ceramic ternary system based on bismuth sodium titanate-bismuth potassium titanate-barium titanate near the morphotropic phase boundary", *Jpn. J. Appl. Phys.*, **42** (2003) 7401–7403.
25. L. Wu, D.Q. Xiao, D.M. Lin, J.G. Zhu, P. Yu, "Synthesis and properties of $[Bi_{0.5}(Na_{1-x}Ag_x)_{0.5}]_{(1-y)}$ Ba_yTiO_3 piezoelectric ceramics", *Jpn. J. Appl. Phys.*, **44** (2005) 8515–8518.
26. A. Herabut, A. Safari, "Processing and electromechanical properties of $(Bi_{0.5}Na_{0.5})_{(1-1.5x)}La_xTiO_3$ ceramics", *J. Am. Ceram. Soc.*, **80** (1997) 2954–2958.
27. H.D. Li, C.D. Feng, P.H. Xiang, "Electrical properties of La^{3+} doped $(Na_{0.5}Bi_{0.5})_{0.94}Ba_{0.06}TiO_3$ ceramics", *Jpn. J. Appl. Phys.*, **42** (2003) 7387–7391.
28. H.D. Li, C. Feng, W. Yao, "Some effects of different additives on dielectric and piezoelectric properties of $(Bi_{1/2}Na_{1/2})TiO_3$–$BaTiO_3$ morphotropic phase boundary composition", *Mater. Lett.*, **58** (2004) 1194–1198.
29. X. Zhou, H.S. Gu, T.Y. Wang, W.Y. Li, T.S. Zhou, "Piezoelectric properties of Mn-doped $(Na_{0.5}Bi_{0.5})_{0.92}Ba_{0.08}TiO_3$ ceramics", *Mater. Lett.*, **59** (2005) 1649–1652.
30. C. Zhou, X. Liu, W. Li, C. Yuan, "Dielectric and piezoelectric properties of Y_2O_3-doped $(Na_{0.5}Bi_{0.5})_{0.94}Ba_{0.06}TiO_3$ ceramics", *Mater. Res. Bull.*, **44** (2009) 724–727.
31. N.A. Hegab, A.E. Bekheet, M.A. Afifi, L.A. Wahaba, H.A. Shehata, "Effect of Cd addition on the A.C. conductivity and dielectric properties of $Ge_{70}Te_{30}$ films", *J. Ovonic. Res.*, **3** [4] (2007) 71–82.
32. J.C. Maxwell, *Electricity and Magnetism*, Vol 1, Oxford, Oxford University Press, Oxford, 1929.
33. C.G. Koops, "On the dispersion of resistivity and dielectric constant of some semiconductors at audio frequencies", *Phys. Rev.*, **83** (1951) 121–124.
34. D.R. Patil, S.A. Lokare, R.S. Devan, S.S. Chougule, C.M. Kanamadi, Y.D. Kolekar, B.K. Chougule, "Studies on electrical and dielectric properties of $Ba_{1-x}Sr_xTiO_3$", *Mater. Chem. Phys.*, **104** (2007) 254–257.
35. K.C. Verma, M. Ram, J. Singh, R.K. Kotnala, "Impedance spectroscopy and dielectric properties of Ce and La substituted $Pb_{0.7}Sr_{0.3}(Fe_{0.012}Ti_{0.988})O_3$ nanoparticles", *J. Alloy. Compd.*, **509** (2011) 4967–4971.
36. D.D. Shah, P.K. Mehta, M.S. Desai, C.J. Panchal, "Origin of giant dielectric constant in $Ba[(Fe_{1-x}Co_x)_{1/2}Nb_{1/2}]O_3$", *J. Alloy. Compd.*, **509** (2011) 1800–1808.
37. A.R. von Hippel, *Dielectrics and Wave*, Wiley, New York, 1954.
38. M.F. Zhang, Y. Wang, K.F. Wang, J.S. Zhu, J.-M. Liu, "Characterization of oxygen vacancies and their migration in Ba-doped $Pb(Zr_{0.52}Ti_{0.48})O_3$ ferroelectrics", *J. Appl. Phys.*, **105** (2009) 061639.
39. W.L. Warren, K. Vanheusden, D. Dimos, G.E. Pike, B.A. Tuttle, "Oxygen vacancy motion in perovskite oxides", *J. Am. Ceram. Soc.*, **79** [2] (1996) 536–538.
40. F.A. Kröger, H.J. Vink, "Relations between the concentrations of imperfections in crystalline solids", *Solid State Phys.*, **3** (1956) 307–435.
41. M.J. Forbess, S. Seraji, Y. Wu, C.P. Nguyen, G.Z. Cao, "Dielectric properties of layered perovskite $Sr_{1-x}A_xBi_2Nb_2O_9$ ferroelectrics (A = La, Ca and x = 0, 0.1)", *Appl. Phys. Lett.*, **76** [20] (2000) 2934–2936.
42. K. Funke, "Jump relaxation in solid electrolytes", *Prog. Solid State Chem.*, **22** [2] (1993) 111–195.
43. S.R. Elliot, "AC conduction in amorphous chalcogenide and pnictide semiconductors", *Adv. Phys.*, **36** (1987) 135–217.
44. Z.W. Chen, Z.Y. Lu, J.Q. Hu, "Piezoelectric and dielectric properties of $(Bi_{0.5}Na_{0.5})_{0.94}$ $(Ba_{1-x}Sr_x)_{0.06}TiO_3$ lead-free piezoelectric ceramics", *Key Eng. Mater.*, **368-372** (2008) 1911–1914.
45. H. Wang, R. Zuo, Y. Liu, J. Fu, "Densification behavior, microstructure, and electrical properties of sol-gel-derived niobium-doped $(Bi_{0.5}Na_{0.5})_{0.94}Ba_{0.06}TiO_3$ ceramics", *J. Mater. Sci.*, **45** (2010) 3677–3682.